Berberine blocks inflammasome activation and alleviates diabetic cardiomyopathy via the miR-18a-3p/Gsdmd pathway

LIN YANG[1*], CHUN-FENG CHENG[1*], ZHI-FANG LI[1], XIAO-JING HUANG[1], SHAO-QING CAI[1], SHAN-YU YE[1], LI-JUN ZHAO[1], YI XIONG[2], DONG-FENG CHEN[3], HE-LU LIU[1], ZHEN-XING REN[4] and HONG-CHENG FANG[1]

[1]Shenzhen Hospital of Integrated Traditional Chinese and Western Medicine, Guangzhou University of Chinese Medicine, Shenzhen, Guangdong 518104; [2]Biomedical Research Institute, The Hong Kong University of Science and Technology Medical Center, Shenzhen Peking University, Shenzhen, Guangdong 518036; [3]Department of Anatomy, School of Basic Medical Sciences, Guangzhou University of Chinese Medicine, Guangzhou, Guangdong 510006; [4]Shanghai Jiao Tong University Affiliated Sixth People's Hospital, Shanghai 200233, P.R. China

Received August 5, 2022; Accepted March 16, 2023

DOI: 10.3892/ijmm.2023.5252

Abstract. Diabetic cardiomyopathy (DCM) is a cardiovascular disease which has been reported as a major cause of mortality worldwide for several years. Berberine (BBR) is a natural compound extracted from a Chinese herb, with a clinically reported anti-DCM effect; however, its molecular mechanisms have not yet been fully elucidated. The present study indicated that BBR markedly alleviated DCM by inhibiting IL-1β secretion and the expression of gasdermin D (Gsdmd) at the post-transcriptional level. Considering the importance of microRNAs (miRNAs/miRs) in the regulation of the post-transcriptional process of specific genes, the ability of BBR to upregulate the expression levels of miR-18a-3p by activating its promoter (-1,000/-500) was examined. Notably, miR-18a-3p targeted Gsdmd and abated pyroptosis in high glucose-treated H9C2 cells. Moreover, miR-18a-3p overexpression inhibited Gsdmd expression and improved biomarkers of cardiac function in a rat model of DCM. On the whole, the findings of the present study indicate that BBR alleviates DCM by inhibiting miR-18a-3p-mediated Gsdmd activation; thus, BBR may be considered a potential therapeutic agent for the treatment of DCM.

Correspondence to: Professor Hong-Cheng Fang, Shenzhen Hospital of Integrated Traditional Chinese and Western Medicine, Guangzhou University of Chinese Medicine, 3 Shajing Street, Bao'an, Shenzhen, Guangdong 518104, P.R. China
E-mail: 13602568079@139.com

Dr Zhen-Xing Ren, Shanghai Jiao Tong University Affiliated Sixth People's Hospital, 600 Yishan Road, Xuhui, Shanghai 200233, P.R. China
E-mail: rzhenxing_168@163.com

*Contributed equally

Key words: berberine, diabetic cardiomyopathy, gasdermin D, pyroptosis, microRNA-18a-3p

Introduction

Diabetic cardiomyopathy (DCM) has been reported as a major cause of morbidity and mortality in cardiomyopathy-related disorders worldwide (1). The prevalence of DCM indicates a parallel ascending trend with obesity and type II diabetes mellitus (2,3). As regards potential treatments for the specific setting of DCM, there is still a lack of effective approaches (4). Therefore, the identification or development of alternative and/or complementary medical treatments for an optimal management scheme of DCM is imperative.

Berberine (BBR) is a bioactive ingredient derived from a common Chinese herb (*Rhizoma coptidis*; known as 'Huang Lian' in Chinese) with application in Traditional Chinese medicine for the treatment of inflammatory disorders and diabetes mellitus-induced cardiovascular injury (5). BBR has demonstrated an optimal clinical and safety profile through extensive pharmacological research (6). In addition to its advantages, it is considered a highly promising nature-derived medicine for the treatment of DCM (7,8). However, the underlying molecular mechanisms of this compound require further investigation.

The programmed cell death known as pyroptosis has been reported to occur during the process of myocardial damage and repair, resulting in collagen deposit accumulation, ultimately forming a collagen-based scar (9). Accumulating evidence has revealed that DCM is associated with pyroptosis (10). The induction of pyroptosis has demonstrated a close association with the heightened activation of the NOD-like receptor 3 (Nlrp3) inflammasome. These multiprotein complexes cleave and transform pro-caspase-1 into the mature and functional caspase-1, which subsequently produces an N-terminal pore-forming fragment (Gsdmd-NT) by cleaving the full-length gasdermin D (Gsdmd-FL) (11). In addition, Gsdmd causes cytolytic membrane rupture and the passive release of pro-inflammatory cytokines, including IL-1β and IL-18 (12,13). Recently, the Nlrp3 inflammasome signaling pathway has been recognized as a main factor contributing to the development of cardiovascular disease (CVD) (14). However, a limited number of studies have addressed the role of pyroptosis in DCM.

MicroRNAs (miRNAs/miRs) are a class of highly evolutionarily conserved non-coding RNAs, which play critical roles in a variety of biological processes and diseases (15,16). Several studies have revealed the involvement of these small (~22 nt) RNA molecules in the cell death and proliferation of cardiomyocytes (17,18). Thus far, miRs are widely recognized as prognostic biomarkers for assessing the development and progression of CVD. Moreover, several miRNA-based therapies are considered promising next-generation management schemes for preventing and treating different diseases, including diabetes and CVD (19,20).

The results of the present study indicate that BBR can effectively prevent myocardial fibrosis by limiting Gsdmd-mediated pyroptosis in a rat model of DCM. The inhibitory effects of BBR on Gsdmd transcription are suggested to be exerted by the upregulation of miR-18a-3p expression. In addition, the results of the present study demonstrate the inhibitory effects of miR-18a-3p on Gsdmd *in vivo* and *in vitro*. Moreover, BBR promotes the activation of the miR-18a-3p promoter, resulting in the upregulation of its expression. In summary, the results of the present study indicate that BBR may suppress pyroptosis via the miR-18a-3p/Gsdmd pathway and exert therapeutic effects against Nlrp3-related inflammatory diseases.

Materials and methods

Animals. A total of 56 male Sprague-Dawley rats (age, 6 weeks; weight, 100-120 g), were purchased from the Hong Kong University of Science and Technology Medical Center, Shenzhen Peking University [SYXK (Yue) 2020-0106]. The animal experimental procedures were performed under the approval of the Experimental Ethics Committee of Hong Kong University of Science and Technology Medical Center, Shenzhen Peking University. The rats were maintained at a constant temperature of 22±2˚C and 40-60% humidity on a 12-h light/dark cycle with free access to standard rodent food and water. They were kept adaptive for breeding for at least 1 week prior to surgery.

Animal model. The rats belonging to the DCM model and control groups received a high-fat diet and a normal diet, respectively, for a period of 4 weeks. Subsequently, the rats were intraperitoneally administered 30 mg/kg streptozotocin (STZ) per day (MilliporeSigma) for 5 consecutive days to induce DCM and were fed a high-fat diet for 4 weeks. The high-fat diet consisted of 66.5% standard laboratory chow, 10% lard, 20% carbohydrate, 2.5% cholesterol, and 1% bile acid sodium (Syagen Biosciences). The control rats were administered a regular diet. The regular diet consisted of 75% corn, 20% wheat bran, 3% fish meal, 1.5% farina and 5% salt (Syagen Biosciences). The successful establishment of the model was confirmed when blood glucose levels ≥11.1 mmol/l were detected in blood acquired from the tail vein, evaluated using a contour glucose meter (Roche Diagnostics).

Animal treatments. A total of 24 rats were randomly divided into three groups (n=8/group) as follows: The control, DCM and DCM treated with BBR (BBR-DCM)groups, as previously described (21). BBR (cat. no. B107342; Shanghai Aladdin Biochemical Technology Co., Ltd.) was dissolved in physiological saline and intragastrically administered daily (200 mg/kg) for a further 4 weeks following the induction of DCM (22). The rats in the control and DCM groups received an equal volume of physiological saline.

In order to evaluate the effects of miR-18a-3p overexpression on the heart functions of diabetic rats, 32 rats (n=8/group) were used for this experiment. The groups used were the following: The control, DCM, scrambled miR (Scm)-DCM and the overexpressing miR-18a-3p (OE-18a-3p)-DCM groups. The rats in the OE-18a-3p-DCM group were generated by an intravenous (i.v.) injection of adeno-associated virus (AAV) overexpressing miR-18a-3p (Shanghai GenePharma Co., Ltd.) for 4 weeks following the induction of DCM. The rats in the Scm-DCM group received AAV containing scrambled miR via i.v. injection. The rats in the control and DCM groups received physiological saline via i.v. injection.

After BBR and AAV intervention, all rats were sacrificed under anesthesia using 30 mg/kg pentobarbital sodium with cervical dislocation, pentobarbital sodium was only used for anesthesia prior to euthanasia. Subsequently, blood samples and mouse hearts were collected. The heart tissues were rapidly frozen in liquid nitrogen and stored at -80˚C or fixed using 4% paraformaldehyde (cat. no. BL539A; Biosharp Life Sciences) at room temperature for 2 h. Humane endpoints were defined for this experiment, including the inability to access food or water, dyspnea, astasia, self-mutilation, a weight loss >15% within 5 days and death was confirmed by breath cessation.

Cells, cell culture and transfection. 293T cells (cat. no. 632180, Takara Bio, Inc.) were cultured in DMEM (cat. no. C11995500BT; Gibco; Thermo Fisher Scientific, Inc.) supplemented with 10% FBS. H9C2 cell (cat. no. CL-0089; Procell Life Science & Technology Co., Ltd.) suspensions containing glucose concentrations of 5.5 mmol/l (control) and 33 mmol/l high glucose (HG) were cultured at 37˚C in the presence of 5% CO_2 for 48 h, as previously described (23). The cells in the culture plates were subsequently transfected with Lipofectamine 3000 (Invitrogen; Thermo Fisher Scientific, Inc.) at 37˚C for 24 h in accordance with the manufacturer's instructions. For this purpose, miR-18a-3p mimics (50 nmol), miR-18a-3p inhibitor (100 nmol), or the negative control (NC); all designed and synthesized by Guangzhou RiboBio Co., Ltd.) were diluted in 200 μl Opti-MEM (Thermo Fisher Scientific, Inc.). Following incubation for 20 min at room temperature, the mixture was added to the cell cultures. The sequences were as follows: miR-18a-3p mimic sense strand, 5'-ACUGCCCUA AGUGCUCCUUCU-3' and antisense strand, 5'-UGACGG GAUUCACGAGGAAGA-3'; miR-18a-3p inhibitor, 5'-AGA AGGAGCACUUAGGGCAUG-3'; NC sense strand, 5'-UUU GUACUACACAAAAGUACUG-3' and antisense strand, 5'-AAACAUGAUGUGUUUUCAUGAC-3'.

Hematoxylin and eosin (H&E) and Masson's trichrome staining. The cardiac tissues were fixed using 4% paraformaldehyde (cat. no. BL539A; Biosharp Life Sciences) at room temperature for 2 h and embedded in paraffin. Subsequently, the tissue samples were sectioned into 5-μm-thick slices and stained with H&E (cat. no. E607318-0200; Sangon Biotech Co., Ltd.) and Masson's (cat. no. G1346; Beijing Solarbio Science & Technology Co., Ltd.) trichrome staining at room

temperature according to the manufacturer's instructions separately. The myocardial histomorphology and collagen deposition were examined using a fluorescence microscope (Cytation 5, BioTek).

Western blotting. Protein extraction from H9C2 cells and cardiac tissues was performed using RIPA lysis buffer (Thermo Fisher Scientific, Inc.) and 100X protease inhibitor cocktail (Thermo Fisher Scientific, Inc.). A BCA protein assay kit was used to determine the protein concentrations (cat. no. P0010S, Beyotime Institute of Biotechnology). Subsequently, 20 μg protein samples were electrophoresed on 10% SDS gels by PAGE. Following protein transfer to polyvinylidene difluoride membranes (0.22 μm; EMD Millipore) and blocking with 5% milk at room temperature for 1 h, the membranes were incubated with primary rabbit anti-β-actin (cat. no. ab49900; 1:20,000; Abcam), rabbit anti-Gapdh (1:10,000; cat. no. ab9482; Abcam), rabbit anti-Nlrp3 (1:1,000; cat. no. NBP2-67639; Novus Biologicals, LLC), mouse anti-caspase-1 (1:2,000; cat. no. NB100-56565; Novus Biologicals, LLC) and rabbit anti-Gsdmd (1:1,000; cat. no. ab209845; Abcam) at 4˚C overnight. On the following day, goat with anti-rabbit antibody (1:20,000; cat. no. ab6276; Abcam) or goat anti-mouse antibody (1:20,000; cat. no. ab6789; Abcam) were applied at room temperature for 1 h. β-actin and Gapdh were used as internal controls. The band visualization was performed using enhanced chemiluminescence (cat. no. WBKLS0500, MilliporeSigma). The densitometry of immunoreactive bands was calculated by ImageJ 1.54b (National Institutes of Health).

RNA extraction and reverse transcription-quantitative PCR (RT-qPCR). Bioinformatics tools were used to predict the Gsdmd-targeting miRNAs (http://www.targetscan.org/, http://www.mirdb.org/, http://www.pictar.org/). Total RNA extraction from cardiac tissues and H9C2 cells was performed using TRIzol™ reagent (Invitrogen; Thermo Fisher Scientific, Inc.). Subsequently, total RNA was converted to cDNA using the Transcriptor First Strand cDNA Synthesis Kit (cat. no. 4897030001; Roche Diagnostics), with a mix of dT primers for mRNA and stem loop primers (Sangon Biotech Co. Ltd.) for miRNA, at 50˚C for 1 h. An Faststart Universal SYBR Green (cat. no. A6001; Promega) was used to perform qPCR with the Bio-Rad CFX96 (Bio-Rad) and Real-Time PCR system. The PCR conditions were 10 min at 95˚C followed by 40 cycles of 95˚C for 15 sec and 60˚C for 1 min. Relative quantification was calculated using the $2^{-\Delta\Delta Ct}$ method (24,25). U6 and β-actin were used as an internal control for the respective miRs and all other mRNAs. The primer sequences used are shown in Table I.

Reactive oxygen species (ROS) evaluation. The cellular content of ROS was evaluated using a dichloro-dihydro-fluorescein diacetate (DCFH-DA) assay kit (Beyotime Institute of Biotechnology). Briefly, the H9C2 cells were seeded at a density of $2x10^5$ cells/plate in six-well plates at 37˚C and incubated for 24 h. The cells were transfected in three groups as follows: The first group was transfected with miR-18a-3p mimics, the second with miR-18a-3p inhibitor, and the third with NC. Subsequently, the cells were cultured with 33 mmol/l HG, and following 48 h, 10 μmol/l DCFH-DA solution were added to the wells. The samples were incubated at 37˚C for 20 min in the dark. Following this incubation, the ROS content of the cells in different groups was evaluated by measuring the fluorescence activity at 495 nm excitation wavelength and 529 nm emission wavelength in real-time (Synergy H1, BioTek).

Dual-luciferase reporter assay. A WT or mut-Gsdmd fragment was constructed and cloned after the luciferase reporter gene of the psiCHECK2 vector (Promega Corporation). Briefly, 293T cells were seeded in 24-well plates, incubated overnight at 37˚C and transfected with Gsdmd WT-vector, Gsdmd Mut-vector by Lipofectamine 3000 (Invitrogen; Thermo Fisher Scientific, Inc.). The cells were then co-transfected with the miR-18a-3p mimic or inhibitor. The relative Firefly and *Renilla* luciferase activity were detected using a dual-luciferase reporter system (cat. no. #E3971; Promega Corporation) at 24 h after transfection. Firefly luciferase served as an internal reference.

The miR-18a-3p promoter fragments (-2,000, -1,500, -1,000 and -500 bp) were synthesized and cloned into the *Xho*I site of the pGL3 vector (Promega Corporation). 293T cells were co-transfected the constructs with the TK vector by Lipofectamine 3000 with or without BBR. The samples were incubated for 24 h at 37˚C. The Firefly and *Renilla* luciferase activity were detected, Firefly luciferase served as an internal reference.

ELISA. The supernatants were collected from all cell cultures and tissue samples, and the released inflammatory cytokine amount in each sample was evaluated using a rat IL-1β ELISA kit (cat. no. ELR-IL1b-1; Raybiotech, Inc.) according to the manufacturer's instructions. The levels of cardiac troponin-I (cTn-I) and creatine kinase-MB (CK-MB) in serum were determined using a Rat Troponin I type 3/cTn-I (cat. no. E-EL-R1253c; Elabscience Biotechnology, Inc.) and a rat CK-MB ELISA kit (cat. no. MM-61468r1; MEIMIAN; http://www.mmbio.cn/goods.php?id=18052), respectively following the manufacturer's instructions. The absorbance was measured at 450 nm (Epoch2, BioTek Instruments, Inc.).

Evaluation of cell death. The cell death rate (pyroptosis) was examined using calcein-AM staining. For this purpose, the cells were initially plated in a six-well plate overnight and subsequently transfected with miR-18a-3p mimics or miR-18a-3p inhibitors for 24 h. Subsequently, the cells were stimulated with HG for an additional 48 h and stained with 5 μM propidium iodide (PI) plus 5 μM calcein-AM for 20 min at 37˚C. The images of non-viable and viable cells were captured by fluorescence microscopy (Cytation 5, BioTek Instruments, Inc.). PI-positive cells revealed the non-viable cells and calcein AM-stained cells represented the viable cells.

Statistical analysis and reproducibility. The obtained data are reported as the mean ± standard error. An unpaired Student's t-test was used for two-group comparisons and one-way analysis of variance (ANOVA) followed by the Tukey's post hoc test was used for multiple group comparisons. Analyses were performed with Prism 7 (Dotmatics). The number of replicates is outlined in the figure legends. $P<0.05$ was considered to indicate a statistically significant difference. All non-significant data are represented as ns throughout the manuscript.

Table I. Primers used for RT-qPCR in the present study.

miR-18a-3p	RT	5'-GTCGTATCCAGTGCAGGGTCCGAGGTATTCGCACTGGATACGACAGAA-3'
	F	5'-CGCGACTGCCCTAAGTGCT-3'
	R	5'-AGTGCAGGGTCCGAGGTATT-3'
miR-20a-3p	RT	5'-GTCGTATCCAGTGCAGGGTCCGAGGTATTCGCACTGGATACGACTGTAAG-3'
	F	5'-CGCGACTGCATTACGAGCA-3'
	R	5'-AGTGCAGGGTCCGAGGTATT-3'
miR-134-5p	RT	5'-GTCGTATCCAGTGCAGGGTCCGAGGTATTCGCACTGGATACGACCCCCTC-3'
	F	5'-CGCGTGTGACTGGTTGACCA-3'
	R	5'-AGTGCAGGGTCCGAGGTATT-3'
miR-146a-3p	RT	5'-GTCGTATCCAGTGCAGGGTCCGAGGTATTCGCACTGGATACGACAAAGAA-3'
	F	5'-GCGCGACCTGTGAAGTTCAG-3'
	R	5'-AGTGCAGGGTCCGAGGTATT-3'
miR-182	RT	5'-GTCGTATCCAGTGCAGGGTCCGAGGTATTCGCACTGGATACGACCGGTGT-3'
	F	5'-GCGTTTGGCAATGGTAGAACTC-3'
	R	5'-AGTGCAGGGTCCGAGGTATT-3'
miR-485-5p	RT	5'-GTCGTATCCAGTGCAGGGTCCGAGGTATTCGCACTGGATACGACGAATTC-3'
	F	5'-CGAGAGGCTGGCCGTGAT-3'
	R	5'-AGTGCAGGGTCCGAGGTATT-3'
miR-544-3p	RT	5'-GTCGTATCCAGTGCAGGGTCCGAGGTATTCGCACTGGATACGACAGCTTG-3'
	F	5'-GCGCGATTCTGCATTTTTAG-3'
	R	5'-AGTGCAGGGTCCGAGGTATT-3'
miR-874-3p	RT	5'-GTCGTATCCAGTGCAGGGTCCGAGGTATTCGCACTGGATACGACTCGGTC-3'
	F	5'-CTGCCCTGGCCCGAGG-3'
	R	5'-AGTGCAGGGTCCGAGGTATT-3'
miR-3084b-3p	RT	5'-GTCGTATCCAGTGCAGGGTCCGAGGTATTCGCACTGGATACGACTTGTCT-3'
	F	5'-GCGCTGCCAGTTCCCTTC-3'
	R	5'-AGTGCAGGGTCCGAGGTATT-3'
miR-3084d	RT	5'-GTCGTATCCAGTGCAGGGTCCGAGGTATTCGCACTGGATACGACTGTCTG-3'
	F	5'-GCGTTCTGCCAGTCCCCTT-3'
	R	5'-AGTGCAGGGTCCGAGGTATT-3'
miR-431	RT	5'-GTCGTATCCAGTGCAGGGTCCGAGGTATTCGCACTGGATACGACTGCATG-3'
	F	5'-GCGTGTCTTGCAGGCCGT-3'
	R	5'-AGTGCAGGGTCCGAGGTATT-3'
miR-3544	RT	5'-GTCGTATCCAGTGCAGGGTCCGAGGTATTCGCACTGGATACGACGGGAAC-3'
	F	5'-CGAACTCCTGCATGACGCC-3'
	R	5'-AGTGCAGGGTCCGAGGTATT-3'
miR-493-5p	RT	5'-GTCGTATCCAGTGCAGGGTCCGAGGTATTCGCACTGGATACGACAATGAA-3'
	F	5'-CGCGTTGTACATGGTAGGCT-3'
	R	5'-AGTGCAGGGTCCGAGGTATT-3'
miR-let7a-2-3p	RT	5'-GTCGTATCCAGTGCAGGGTCCGAGGTATTCGCACTGGATACGACGGAAAG-3'
	F	5'-CGCGCTGTACAGCCTCCTAG-3'
	R	5'-AGTGCAGGGTCCGAGGTATT-3'
miR-let7g-3p	RT	5'-GTCGTATCCAGTGCAGGGTCCGAGGTATTCGCACTGGATACGACGCAAGG-3'
	F	5'-CGCGCTGTACAGGCCACTG-3'
	R	5'-AGTGCAGGGTCCGAGGTATT-3'
miR-193a-5p	RT	5'-GTCGTATCCAGTGCAGGGTCCGAGGTATTCGCACTGGATACGACTCATCT-3'
	F	5'-GGGGTCTTTGCGGGCA-3'
	R	5'-AGTGCAGGGTCCGAGGTATT-3'
U6	RT	5'-GTCGTATCCAGTGCAGGGTCCGAGGTATTCGCACTGGATACGACAAAATA-3'
	F	5'-AGAGAAGATTAGCATGGCCCCTG-3'
	R	5'-ATCCAGTGCAGGGTCCGAGG-3'
pre-Gsdmd	F	5'-TCTCCACCGTTAGCCCAGAG-3'
	R	5'-GGCATGGGACAGACAACCTG-3'

Table I. Continued.

mature-Gsdmd	F	5'-CTGCTTGCCGTACTCCATTCCATC-3'
	R	5'-TCCCTGATTACTTCTTCCTCATTGGTTC-3'
Nlrp3	F	5'-AGACAGCCTTGAAGAGGAGTGGATAG-3'
	R	5'-AACCTGCTTCTCACATGCCTTCTG-3'
Caspase-1	F	5'-AAACACCCACTCGTACACGTCTTG-3'
	R	5'-AGGTCAACATCAGCTCCGACTCTC-3'
β-actin	F	5'-TGTCACCAACTGGGACGATA-3'
	R	5'-GGGGTGTTGAAGGTCTCAAA-3'

F, forward; R, reverse; Gsdmd, gasdermin D; Nlrp3, NOD-like receptor 3.

Results

Berberine alleviates DCM by inhibiting pyroptosis. To determine whether BBR can ameliorate myocardial injury in DCM, rats with DCM were treated with this compound (Fig. 1A). The expression levels of cardiac biomarkers, including cTn-I and CK-MB were increased in the DCM model group rats and were reduced in the rats in the BBR-treated group, indicating that BBR may exert a cardioprotective effect (Fig. 1B and C). Moreover, the pathological changes of the cardiomyocytes were assessed using H&E staining and collagen deposition was assessed using Masson's staining. The results indicated that the cardiomyocytes in the rats with DCM contained a highly increased number of vacuoles with a disordered arrangement and distortions, which indicated an extensive destruction in the myocardial structures of these models. By contrast, reduced pathological manifestations were observed in the myocardial tissue of the BBR-treated animals compared with those in the DCM group (Fig. 1D). Masson's staining indicated that collagen deposition was increased in the rats with DCM, while it was reduced in the BBR-treated rats (Fig. 1E).

To explore the effects of BBR on pyroptosis, the expression levels of pyroptosis-related proteins and inflammatory cytokines were evaluated. According to the results of western blotting for Nlrp3, caspase-1 and Gsdmd, a significant increase was observed in the expression levels of these proteins in the rats with DCM. BBR suppressed the Gsdmd levels, whereas it had no marked effect on the expression levels of Nlrp3 and caspase-1 (Fig. 1F and G). The expression levels of inflammation-related proteins were investigated using ELISA. The data indicated that the expression levels of IL-1β were increased and this increase was blocked in the BBR-treated rats (Fig. 1H). These data revealed that BBR protected cells from pyroptosis through the obstruction of Gsdmd expression and the release of IL-1β in rats with DCM. To further investigate the mechanisms through which BBR regulates Gsdmd expression, the expression levels of the precursor mRNA (pre-mRNA) and the mature mRNA (mat-mRNA) of Gsdmd were assessed. The results indicated that the expression levels of mat-mRNA of Gsdmd were significantly enhanced and inhibited by BBR (Fig. 1I). However, no significant difference was noted in the expression levels of pre-mRNA in the DCM and BBR-DCM groups (Fig. 1J), which suggested that BBR did not affect the transcription of Gsdmd. Taken together, these data indicated that the downregulation of Gsdmd expression in the BBR-DCM group may be attributed to a post-transcriptional regulation.

miR-18a-3p specifically targets Gsdmd. miRNAs have been demonstrated to regulate gene expression through a post-transcriptional mechanism of action (26). Herein, the effects of BBR were examined on Gsdmd expression by measuring the expression levels of major miRNAs targeting Gsdmd. These Gsdmd-targeting miRs were predicted using TargetScan, miRDB and PicTar prediction servers (http://www.targetscan.org/, http://www.mirdb.org/, http://www.pictar.org/). Subsequently, the results of RT-qPCR demonstrated that the expression of five miRNAs, including miR-18a-3p, miR-134-5p, miR-182, miR-485-5p and miR-3084b-3p was significantly attenuated in the H9C2 cells treated with HG (Fig. 2A). Among these, the expression of miR-18a-3p was dose-dependently upregulated by BBR (Fig. 2B), indicating that it may be crucially involved in the mechanisms of action of BBR. Specifically, the expression levels of miR-18a-3p were significantly decreased in rats with DCM in comparison with the control group, whereas they were increased in the BBR-treated rats compared to the rats with DCM (Fig. 2C).

To further evaluate the possible role of decreased miR-18a-3p levels in the increased expression of Gsdmd, miR-18a mimic and inhibitor were transfected into H9C2 cells. The results revealed that the expression of miR-18a-3p was significantly increased in the miR-18a-3p mimic group and decreased in the miR-18a-3p inhibitor group compared with that in the negative control cells (Fig. 2D). A bioinformatics analysis was applied to analyze the potential targets of miR-18a-3p, which indicated that miR-18a-3p was a potential regulator targeting the Gsdmd 3' untranslated region (UTR) binding sites (Fig. 2E). The Gsdmd 3'UTR with wild-type (WT) or the base-pair mutant miR-18a-3p binding regions were cloned into the psiCHECK2 luciferase reporter to determine whether the miR-18a-3p binds directly to the 3'UTR of Gsdmd. The luciferase activity of the clones expressing the WT miR-18a-3p binding regions was markedly decreased when it was co-transfected with miR-18a-3p mimics and increased in the inhibitor co-infected group, but not in the mutant reporter (Fig. 2F).

In addition, RT-qPCR and western blotting confirmed that the expression levels of Gsdmd in the miR-18a-3p mimic-infected H9C2 cells were decreased as compared with Gsdmd expression in the control group. In addition, Gsdmd expression was increased following transfection of the cells

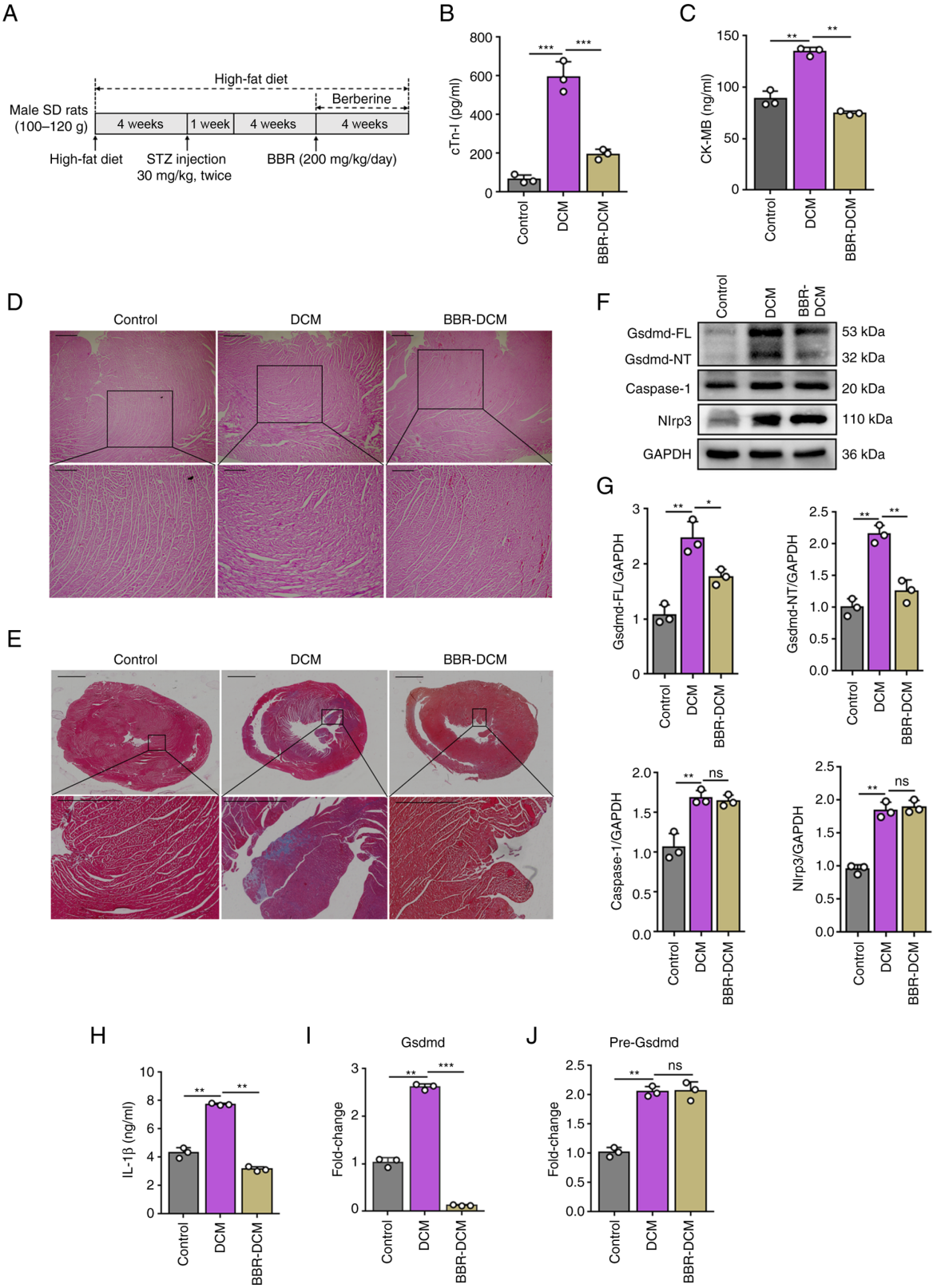

Figure 1. BBR alleviates DCM by inhibiting pyroptosis. (A) The timeline of the animal experiments (n=8/group). (B) cTn-I levels and (C) the CK-MB concentration in the serum samples of BBR-treated rats compared with those in the DCM group and control rats were determined using ELISA. (D) Hematoxylin and eosin stained sections of heart tissues in control or DCM rats treated with or without BBR. Scale bars: Upper panels, 500 μm; lower panels, 200 μm. (E) Masson's trichrome staining was performed on the heart tissue sections derived from rats with DCM treated with or without BBR for 4 weeks, or the control group, respectively. Scale bars: Upper panels, 3,000 μm; lower panels, 1,000 μm. (F and G) Representative western blots and quantification of Gsdmd, caspase-1 and Nlrp3 proteins. Gapdh was used as the loading control. (H) The lysis supernatant of the heart tissue was used for the detection of IL-1β using an IL-1β ELISA kit. (I-J) The mRNA expression levels of mat (I) and pre (J) Gsdmd were assessed using reverse transcription-quantitative PCR, using Gapdh as the loading control. The data in (D-F) are representative of three individual experiments with similar results. The data in (B, C and G-J) are representative of the mean ± SEM. One-way ANOVA followed by Tukey's multiple comparison tests was performed. *P<0.05, **P<0.01 and ***P<0.001. ns, not significant. BBR, berberine; DCM, diabetic cardiomyopathy; cTn-I, cardiac troponin-I; CK-MB, creatine kinase-MB; Gsdmd, gasdermin D; Gsdmd-FL, full length Gsdmd; Gsdmd-NT, Gsdmd N-terminal fragment; Nlrp3, NOD-like receptor 3; mat-, mature; pre-, precursor.

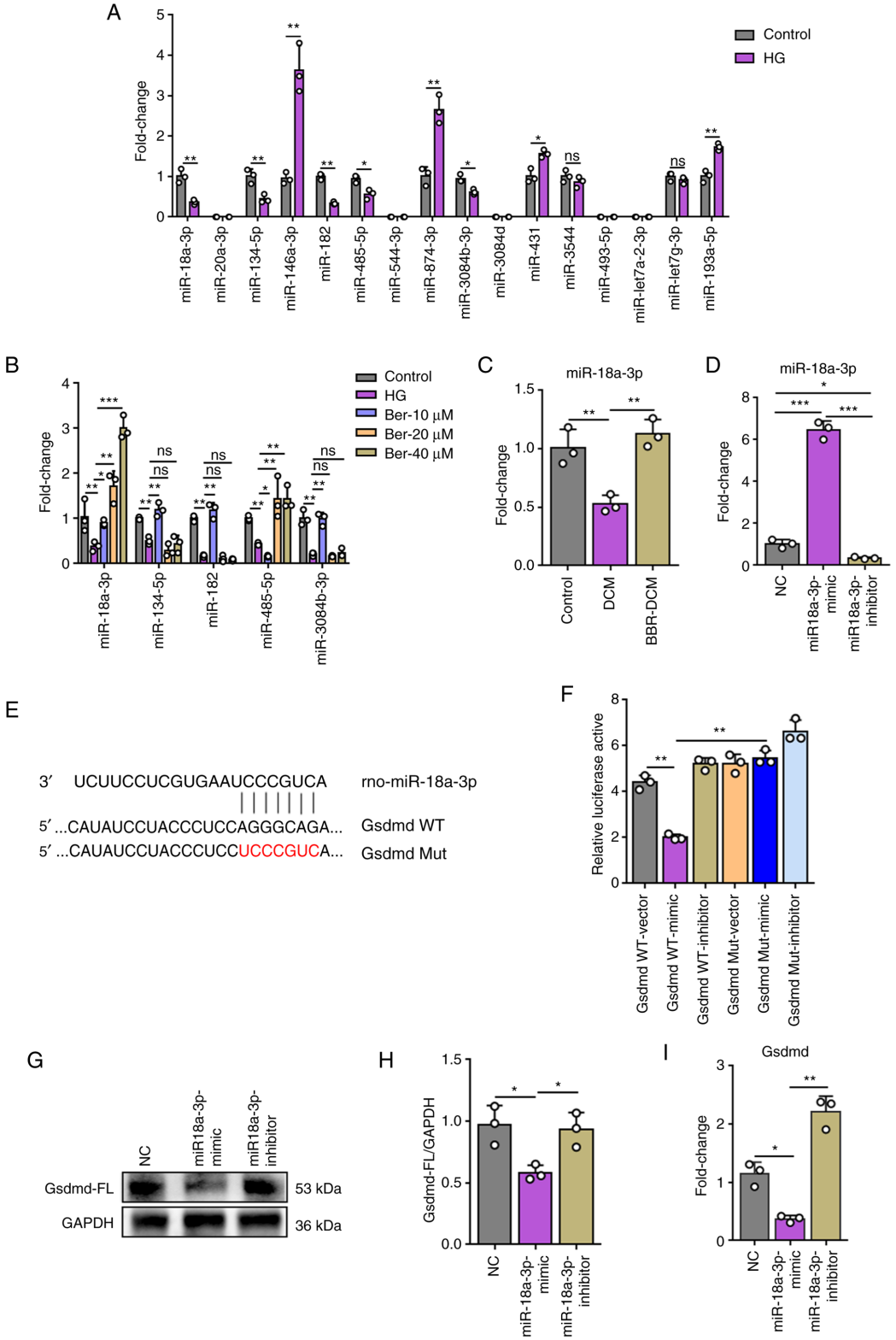

Figure 2. miR-18a-3p specifically targets Gsdmd. (A) H9C2 cells were treated with or without 33 mM HG for 2 days, and the expression levels of the miRs were determined using RT-qPCR. (B) H9C2 cells were incubated with HG (33 mM) for 48 h in the presence or absence of BBR, and miR expression levels were measured using RT-qPCR, with U6 as the loading control. (C) The expression levels of miR-18a-3p in the heart tissues of the rats were measured using RT-qPCR. U6 was used as the loading control. (D) Expression of miR-18a-3p in cells transfected with miR-18a-3p mimic, miR-18a-3p inhibitor and the negative control cells. (E) The miR-18a-3p target sites in the 3'UTR of Gsdmd mRNA were predicted using TargetScan. (F) Luciferase activity was measured following co-transfection with the WT or the MUT version of the Gsdmd luciferase reporter plasmid into 293T cells together with miR-18a-3p mimics or inhibitor and/or the corresponding control. (G-I) H9C2 cells were transfected with miR-18a-3p mimics and inhibitor. The (G and H) protein and (I) mRNA expression levels of Gsdmd were detected using western blotting and RT-qPCR. The data in (G) are representative of three individual experiments. The data in (A-D, F-I) are presented as the mean ± SEM. An unpaired Student's t-test was performed for (A), *P<0.05 and **P<0.01 compared with the control group. One-way ANOVA followed by Tukey's multiple comparison tests was performed for (B-D and F-I). *P<0.05, **P<0.01 and ***P<0.001 compared with the HG group in (B); **P<0.01 as compared with the DCM group in (C); **P<0.01 and ***P<0.001 compared with Gsdmd WT-mimics group in (F); *P<0.05 and **P<0.01 compared with miR-18a-3p mimics group in (H and I). ns, not significant. miR, microRNA; Gsdmd, gasdermin D; HG, high glucose; RT-qPCR, reverse transcription-quantitative PCR; BBR, berberine; 3'UTR, 3' untranslated region; WT, wild-type; MUT, mutant-type; SEM, standard error of the mean.

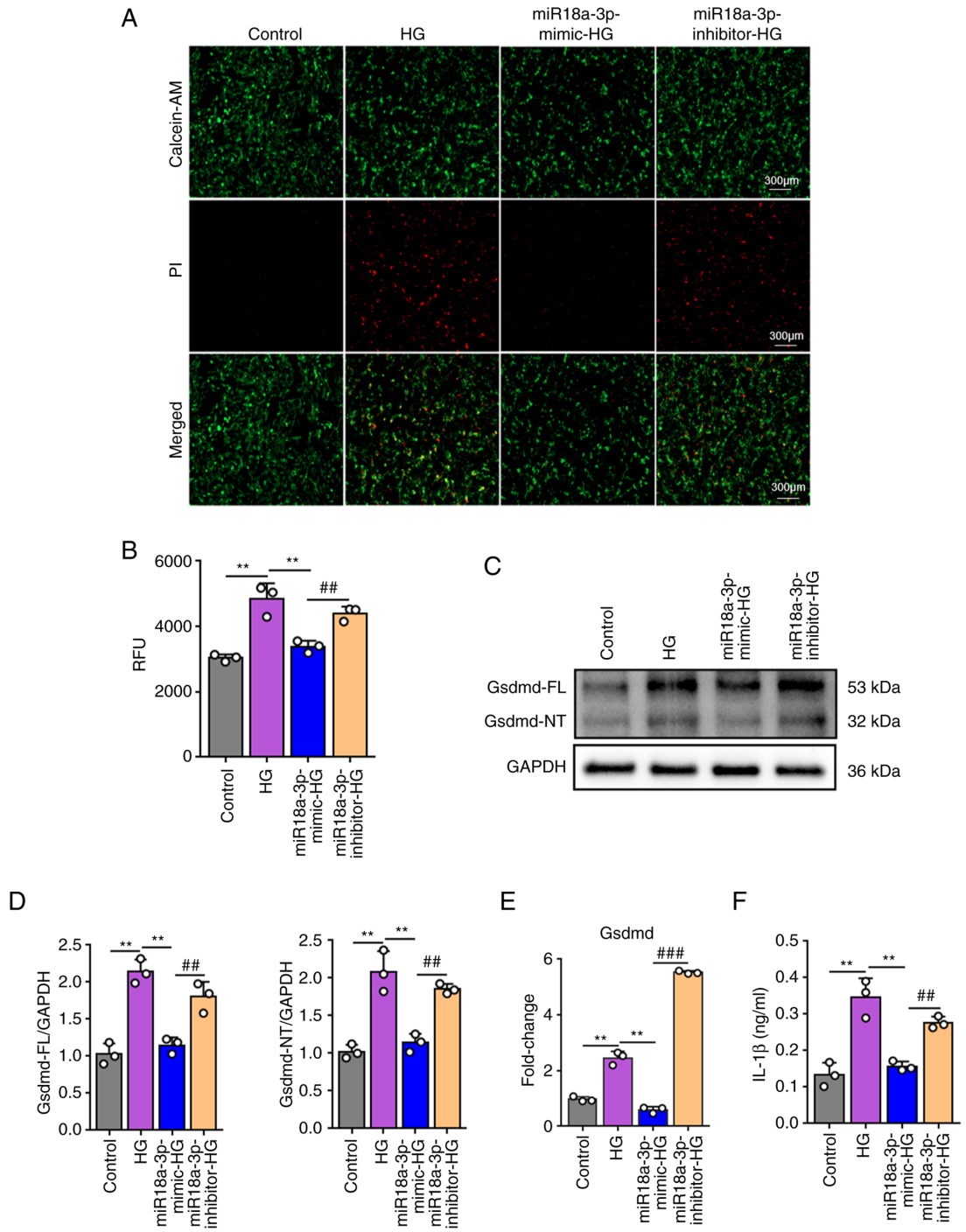

Figure 3. miR-18a-3p reduces Gsdmd expression in HG-treated H9C2 cells. (A) H9C2 cells were transfected with miR-18a-3p mimics and inhibitor for 24 h. Subsequently, they were treated with 33 mM HG for 2 days and the representative immunofluorescence images of viable and non-viable cells were obtained. The non-viable cells were detected by PI (red) and the viable cells were detected by calcein AM (green). Scale bar, 300 μm. (B) The levels of ROS were determined by DCFH-DA-based fluorescence detection. (C and D) The protein and (E) mRNA expression levels of Gsdmd were assessed using western blotting and reverse transcription-quantitative PCR. (F) The release of IL-1β in the supernatants was analyzed using ELISA. The data in (A and C) are representative of three individual experiments with similar results. The data in (B and D-F) are presented as the mean ± SEM. One-way ANOVA followed by Tukey's multiple comparison tests was performed. **P<0.01 compared with the HG group; $^{\#\#}$P<0.01 and $^{\#\#\#}$P<0.001 compared with the miR-18a-3p-mimics-HG group. miR, microRNA; Gsdmd, gasdermin D; HG, high glucose; PI, propidium iodide; ROS, reactive oxygen species; DCFH-DA, dichloro-dihydro-fluorescein diacetate; SEM, standard error of the mean.

with a miR-18a-3p inhibitor (Fig. 2G-I). These findings suggested that the inhibitory effects of miR-18a-3p on Gsdmd are mediated by direct interaction with its 3'UTR terminal.

miR-18a-3p reduces Gsdmd expression in HG-treated H9C2 cells. Considering the regulatory role of ROS in cell growth, pyroptosis, inflammation, fibrosis and even heart failure, the total ROS levels were measured in the cells (27). The results of DCFH-DA-based fluorescence detection indicated that the ROS levels were significantly increased in the HG-treated groups, whereas their production was downregulated by transfection with miR-18a-3p mimics (Fig. 3B). The results of the

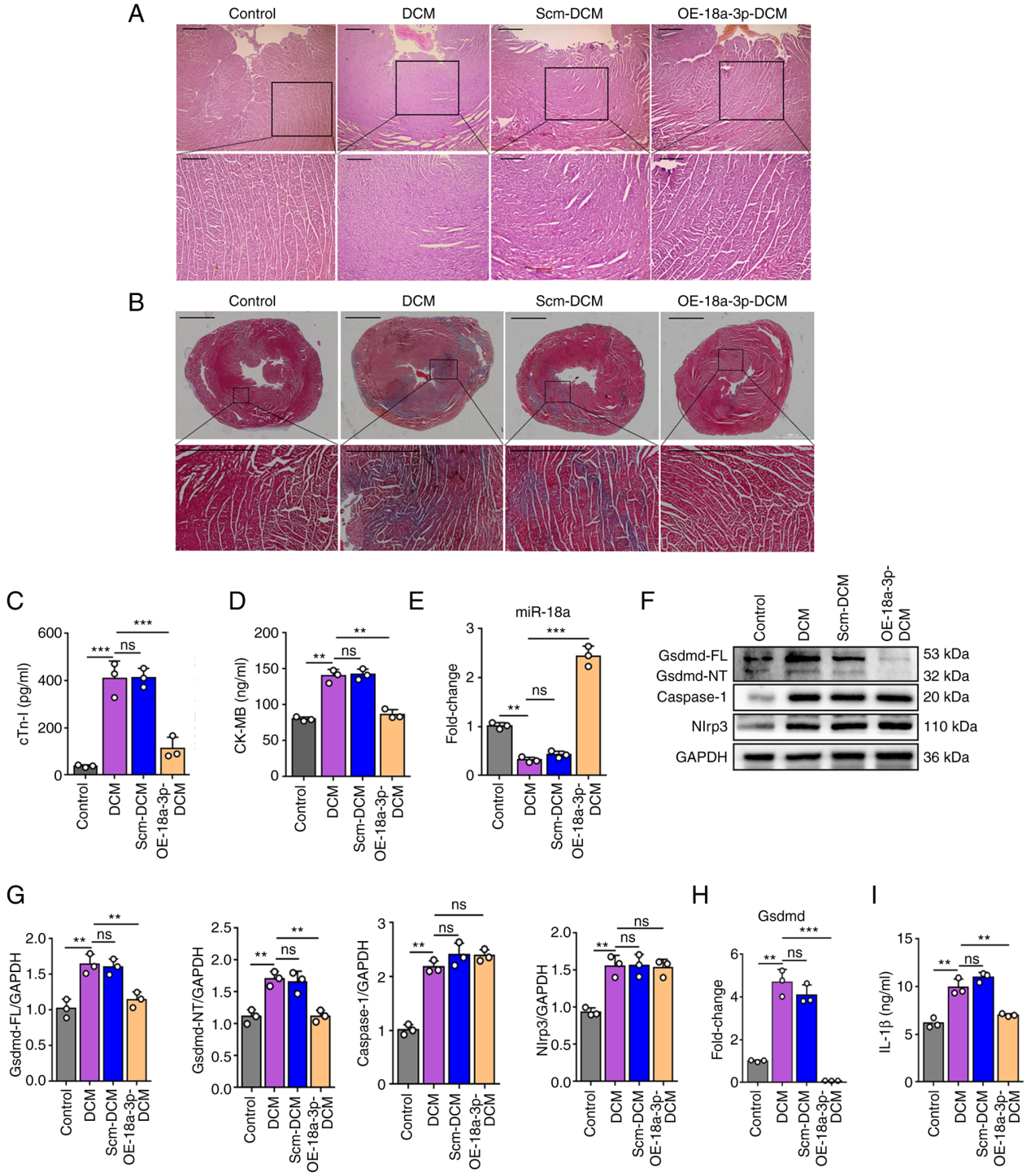

Figure 4. miR-18a-3p alleviates DCM by inhibiting pyroptosis; n=8 rats/group. (A) Hematoxylin and eosin and (B) Masson's trichrome staining of the heart tissues of rats infected with vector/OE-miR-18a-3p adeno-associated virus for 30 days, or of the control group, respectively. (A) Scale bars: Upper panels, 500 μm; lower panels, 200 μm; (B) scale bars: upper panels, 3,000 μm; lower panels, 1,000 μm. (C) cTn-I levels and (D) CK-MB concentration in rat serum overexpressing miR-18a-3p compared with those of the DCM model. The levels of these markers were determined in Scm, DCM and control group rats using ELISA. (E) The transcript levels of miR-18a-3p were measured using RT-qPCR. U6 served as a loading control. (F and G) Representative western blots and quantification of Gsdmd, caspase-1 and Nlrp3 proteins. Gapdh served as the loading control. (H) The mRNA levels of Gsdmd in rats were determined using RT-qPCR. Gapdh served as a loading control. (I) The lysate in the supernatant of the heart tissues was used to evaluate IL-1β levels using ELISA. The data in (A, B and G) are representative of three individual experiments with similar results. The data in (C-F, and H and I) are presented as the mean ± SEM. One-way ANOVA, followed by Tukey's multiple comparison post hoc test was performed. **P<0.01 and ***P<0.001, compared with the vector-DCM group. miR, microRNA; DCM, diabetic cardiomyopathy; OE, overexpressing; cTn-I, cardiac troponin-I; CK-MB, creatine kinase-MB; RT-qPCR, reverse transcription-quantitative PCR; Gsdmd, gasdermin D; Nlrp3, NOD-like receptor 3.

viable/non-viable cell staining revealed that the percentage of HG-induced cells (red) was increased following HG treatment and it was downregulated by miR-18a-3p mimics (Fig. 3A).

To identify whether miR-18a-3p regulates Gsdmd expression, the mRNA and protein levels of Gsdmd were measured. The expression levels of Gsdmd were significantly increased in

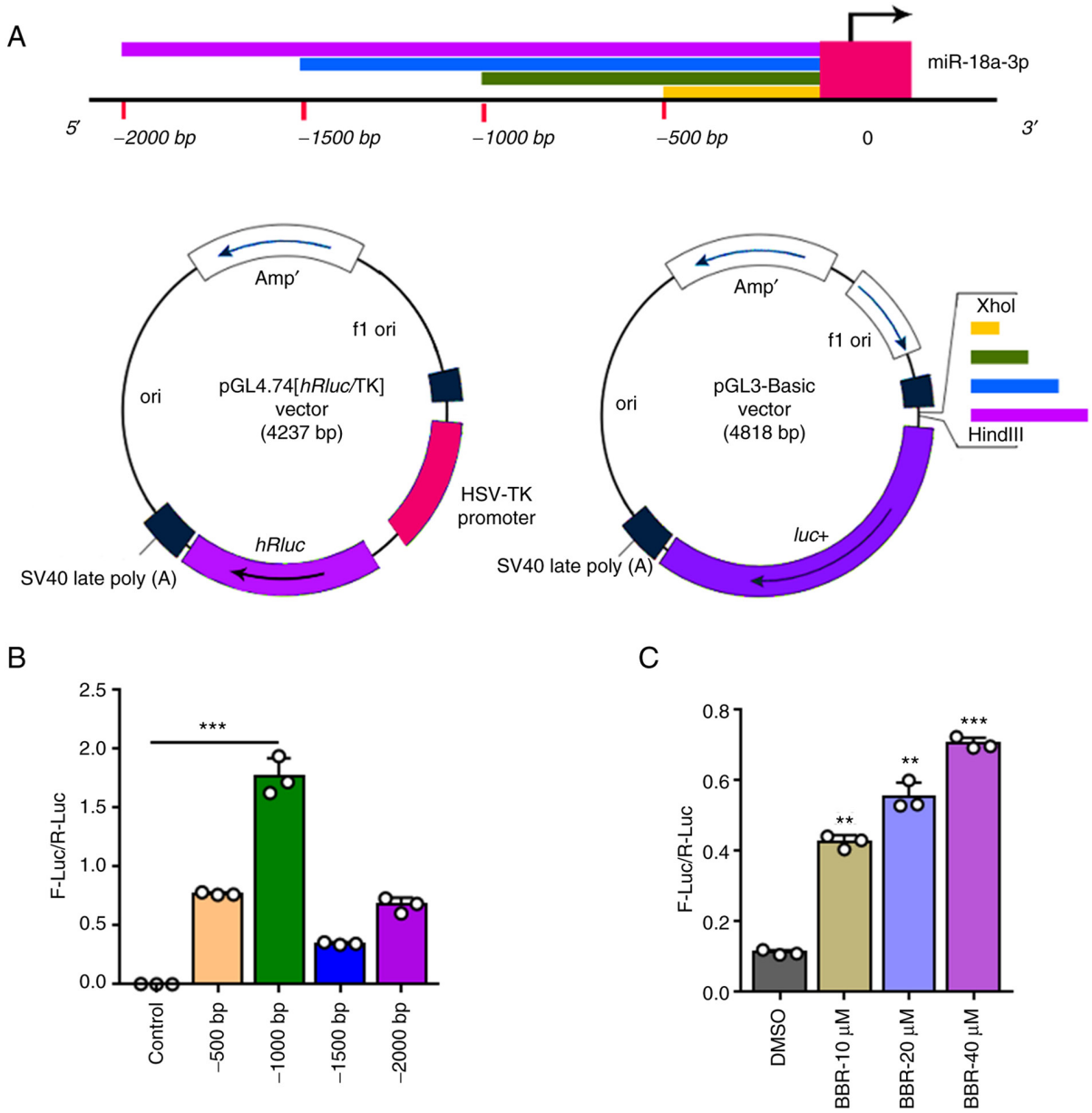

Figure 5. BBR enhances the activation of the miR-18a-3p promoter. (A) Schematic diagram of miR-18a-3p promoter reporters. The 2,000 nt DNA sequence of the promoter segment and a series of deleted fragments were inserted into the dual-luciferase reporter plasmid to promote the miR-18a-3p promoter-reporter. (B) The luciferase reporter plasmids were transfected into 293T cells and the luciferase activity was evaluated. (C) 293T cells were transfected with the 1,000 nt fragment reporter plasmid and incubated with BBR. Subsequently, the luciferase activity was measured. The data in (B and C) are presented as mean ± SEM combined from three independent experiments. One-way ANOVA, followed by Tukey's multiple comparisons post hoc test was performed. **P<0.01 and ***P<0.001 compared with the control group. BBR, berberine; miR, microRNA; SEM, standard error of the mean.

the HG-treated cells and were reduced following transfection with miR-18a-3p mimics (Fig. 3C-E). Moreover, the results of ELISA indicated that the HG-induced cells expressed high levels of IL-1β. miR-18a-3p suppressed the release of IL-1β into the supernatant of H9C2 cells treated with HG (Fig. 3F). According to these results, miR-18a-3p reduced Gsdmd expression and protected the cells from pyroptosis.

miR-18a-3p suppresses Gsdmd expression in vivo. In order to identify whether miR-18a-3p can ameliorate cardiac trauma in DCM *in vivo*, the rats with DCM were subjected to an injection of AAV to overexpress miR-18a-3p or scrambled miR. RT-qPCR analysis revealed that miR-18a-3p was increased in the OE-18a-3p group compared with the DCM group, which indicated that the miRNA-18a-3p was successfully overexpressed in the heart tissues of the rats (Fig. 4E). The results of H&E and Masson's staining indicated that the pathological process of the heart tissues was alleviated compared with the DCM model rats; in addition, collagen deposition was reduced in the rats in the OE-miR-18a-3p group (Fig. 4A and B). Moreover, the expression levels of cTn-I and CK-MB were elevated in the rats with DCM compared with those of the control rats. miR-18a-3p overexpression markedly decreased the levels of these cardiac biomarkers (Fig. 4C and D).

Subsequently, the efficiency of miR-18a-3p in inhibiting Gsdmd expression was investigated in DCM model rats. Following miR-18a-3p overexpression in the cardiac tissue,

the mRNA and protein levels of Gsdmd were decreased compared with those of the model group (Fig. 4F-H). By contrast, miR-18a-3p overexpression indicated the absence of a significant effect on caspase-1 and Nlrp3 expression levels, as compared with those of the DCM model rats (Fig. 4G). Moreover, the expression level of IL-1β was investigated in heart tissues, and it was observed that miR-18a-3p inhibited IL-1β expression (Fig. 4I). In summary, miR-18a-3p partially suppressed Gsdmd expression and IL-1β production *in vivo*, demonstrating that it may be considered as a promising candidate for developing targeted therapeutics for DCM.

BBR enhances the activation of the miRNA-18a-3p promoter. The regulatory effect of BBR on miR-18a-3p expression was assessed by activating its promoter using a dual-luciferase reporter assay. To explore the promoter active region, the authors concentrated on the region 2,000 bp upstream of the transcription start site (TSS) of miR-18a-3p. For confirmation and identification of the core promoter region, a 2,000 bp 5' upstream promoter sequence and multiple deleted fragments of this sequence were constructed using the pGL3-Basic vector, which was subsequently transfected into 293T cells (Fig. 5A). The luciferase activity of these cells was assessed. The results demonstrated that the luciferase activity was significantly increased in the fragment of 1,000/500 bp group compared with that of the control, which suggested that the core promoter was in the -1,000 to -500 BP region relative to the ATG start codon (Fig. 5B). The regulatory function of BBR on the miR-18a-3p promoter was assessed by a luciferase construct containing the miR-18a-3p promoter fragment (-1,000/500 bp), which was co-transfected with BBR in 293T cells. The results indicated an enhanced miR-18a-3p promoter activity at a BBR concentration-independent manner (Fig. 5C), suggesting that BBR enhanced the luciferase activity of the miR-18a-3p promoter.

Discussion

In the present study, the efficacy of BBR in the treatment of DCM was investigated. According to the results reported, BBR effectively decreased myocardial fibrosis by limiting Gsdmd-driven pyroptosis in rats with DCM. As regards the mechanisms of action, the data indicated that BBR exerted an inhibitory effect on Gsdmd transcription by upregulating the expression of miR-18a-3p. These data confirmed that miR-18a-3p exerted a negative regulatory effect on Gsdmd expression that was directly targeted by miR-18a-3p. Moreover, miR-18a-3p overexpression partly alleviated myocardial fibrosis *in vivo*. In addition, BBR increased miR-18a-3p expression levels by promoting the activation of its promoter. Collectively, the findings of the present study indicated the mechanism of BBR action and suggested that the miR-18a-3p/Gsdmd pathway may be used as a diagnostic and therapeutic target for DCM.

BBR is a promising candidate for the therapy of DCM. Previously, the therapeutic effect of BBR was assessed using high sucrose and rats with HFD/STZ-induced DCM. It was demonstrated that BBR considerably prevented diastolic/systolic dysfunction, as well as cardiac hypertrophy in these models (28). Moreover, a previous study indicated that the treatment of diabetic rats with BBR partially improved cardiac function and reduced the levels of fasting blood glucose, total cholesterol, and triglycerides (29). Similarly, the present study indicated that BBR treatment improved cardiac fibrosis and dysfunction in the rat model of DCM.

The role of BBR on HG stimulation has been extensively investigated. It has been demonstrated that in diabetic rats, BBR can activate the cardiac 5'AMP-activated protein kinase and AKT and inhibit GSK3β activity levels (29). Moreover, BBR can elevate the expression levels of the alpha-myosin heavy chain (MHC) and lower the expression levels of the heavy chain of the β-MHC protein in the H9C2 cell hypertrophy model induced by palmitate (30). A previous study found that the expression levels of pro-inflammatory cytokines, including IL-1β, were decreased by BBR via the NF-κB pathway (31). The findings of the present study were consistent with these observations and indicated the inhibition of IL-1β secretion in HG-stimulated H9C2 cells treated with BBR. The Nlrp3 inflammasome is a cytosolic multiprotein complex composed of Nlrp3 and pro-caspase-1. Nlrp3 is released and results in the recruitment of pro-caspase-1, thus promoting autocleavage and activation. Active caspase-1 can cleave Gsdmd and release its N-terminal domain and facilitate the release of IL-1β, contributing to homeostatic maintenance (32). In the present study, BBR notably inhibited the expression levels of Gsdmd under HG treatment conditions, without inhibiting the Nlrp3 and caspase-1 expression levels, suggesting that the inhibition of Gsdmd-mediated pyroptosis was involved in the negative regulatory effect of BBR on IL-1β production. However, the results of RT-qPCR assay indicated that BBR did not exert an effect on the expression levels of pre-mRNA of *Gsdmd*, suggesting that the BBR regulation of mRNA was not at the transcriptional level, probably transpiring at a post-transcriptional stage.

miRs are key regulators in a variety of biological processes and play a critical role in the regulation of mRNA expression (33). The results of the present study also revealed that BBR triggered Gsdmd mRNA transcription through miR-18a-3p binding with the 3'UTR of mRNA. Recently, a study suggested that miR-18a-5p was regulated by N6-methyladenosine RNA methylation for controlling angiogenic responses in endothelial cells (34). Nandi *et al* (35) revealed that miR-18a-5p targeted hypoxia inducible factor-1α to produce mitochondrial abnormalities resulting in cardiomyopathy. However, the crucial role of miR-18a-3p in DCM has not been reported to date. The results of the present study also indicated that the luciferase activity was significantly decreased following transfection of the cells expressing WT-Gsdmd with miR-18a-3p mimics, whereas the mutated Gsdmd 3'UTR within the binding site of the miR-18a-3p seed sequence eliminated the responsiveness to miR-18a-3p. The data further indicated that miR-18a-3p reduced the levels of ROS and cell death rate by suppressing Gsdmd production *in vitro* and *in vivo*. These data collectively suggest that BBR can potentiate miR-18a-3p expression to a certain extent and limit Gsdmd expression and pyroptosis.

The transcriptional mechanism responsible for the effects of BBR on miR-18a-3p has not been extensively investigated. A previous study indicated that BBR reduced hepatic steatosis through its inhibitory effect on the stearoyl-CoA desaturase-1 promoter (36). In the present study, it was found that the core

region of the miR-18a-3p promoter was located between -1,000 and -500 bp relative to the ATG start codon (part of the 500 bp segment). Subsequently, it was hypothesized that BBR regulated the miR-18a-3p promoter transcriptional activity. This hypothesis was confirmed by the concentration-dependent promoting effect of BBR on the miR-18a-3p promoter transcriptional activity. These findings indicate that BBR can transcriptionally regulate the expression levels of miR-18a-3p via a transcriptional mechanism.

A limitation of the present study was that cardiac function biomarkers, including cTn-I, CK-MB were applied to evaluate the cardiac function without directly evaluating cardiac function. In future studies, the authors aim to apply echocardiography in order to analyze cardiac function in animals.

In conclusion, *in vitro* and *in vivo* evidence demonstrating that BBR inhibits the Gsdmd pore formation to alleviate DCM was provided in the present study. Moreover, the results indicated that BBR may enhance the activation of the miR-18a-3p promoter and enhance the expression levels of miR-18a-3p. Therefore, BBR treatment may be considered as a useful therapeutic strategy for decreasing Gsdmd expression. Moreover, targeting the miR-18a-3p/Gsdmd pathway may be used for the successful treatment of Gsdmd-driven diseases, including cardiovascular conditions, diabetes type II, Parkinson's disease and cancer.

Acknowledgements

Not applicable.

Funding

The present study was supported by the China Postdoctoral Science Foundation (grant no. 2021M700961), the Sanming Project of Medicine in Shenzhen (grant no. SZZYSM 202106006), the Bao'an TCM Development Foundation (grant no. 2020KJCX-KTYJ-136) and the National Administration of Traditional Chinese Medicine (grant no. GZY-FJS-2022-60).

Availability of data and materials

The datasets used and/or analyzed during the current study are available from the corresponding author on reasonable request.

Authors' contributions

HCF and ZXR designed the study. LY, CFC and ZFL were responsible for the acquisition of the data. XJH, SQC, LJZ and YX performed the animal experiments. SQC and SYY interpreted the results of the cell culture experiments. LY, DFC and HLL analyzed the data and wrote the manuscript. HCF and ZXR confirm the authenticity of all the raw data. All authors have read and approved the final manuscript.

Ethics approval and consent to participate

The animal study was reviewed and approved by The Animal Ethics Committee of the Hong Kong University of Science and Technology Medical Center, Shenzhen Peking University [Approval no. SYXK (Yue) 2020-0106].

Patient consent for publication

Not applicable.

Competing interests

The authors declare that they have no competing interests.

References

1. Dillmann WH: Diabetic cardiomyopathy: What is it and can it be fixed? Circ Res 124: 1160-1162, 2019.
2. Jia G, Whaley-Connell A and Sowers JR: Diabetic cardiomyopathy: A hyperglycaemia- and insulin-resistance-induced heart disease. Diabetologia 61: 21-28, 2018.
3. Jia G, DeMarco VG and Sowers JR: Insulin resistance and hyperinsulinaemia in diabetic cardiomyopathy. Nat Rev Endocrinol 12: 144-153, 2016.
4. Paolillo S, Marsico F, Prastaro M, Renga F, Esposito L, De Martino F, Di Napoli P, Esposito I, Ambrosio A, Ianniruberto M, *et al*: Diabetic cardiomyopathy: Definition, diagnosis, and therapeutic implications. Heart Fail Clin 15: 341-347, 2019.
5. Feng X, Sureda A, Jafari S, Memariani Z, Tewari D, Annunziata G, Barrea L, Hassan STS, Šmejkal K, Malaník M, *et al*: Berberine in cardiovascular and metabolic diseases: From mechanisms to therapeutics. Theranostics 9: 1923-1951, 2019.
6. Imenshahidi M and Hosseinzadeh H: Berberine and barberry (*Berberis vulgaris*): A clinical review. Phytother Res 33: 504-523, 2019.
7. Pang B, Zhao LH, Zhou Q, Zhao TY, Wang H, Gu CJ and Tong XL: Application of berberine on treating type 2 diabetes mellitus. Int J Endocrinol 2015: 905749, 2015.
8. Zhang Y, Gu Y, Ren H, Wang S, Zhong H, Zhao X, Ma J, Gu X, Xue Y, Huang S, *et al*: Gut microbiome-related effects of berberine and probiotics on type 2 diabetes (the PREMOTE study). Nat Commun 11: 5015, 2020.
9. Wang J, Deng B, Liu Q, Huang Y, Chen W, Li J, Zhou Z, Zhang L, Liang B, He J, *et al*: Pyroptosis and ferroptosis induced by mixed lineage kinase 3 (MLK3) signaling in cardiomyocytes are essential for myocardial fibrosis in response to pressure overload. Cell Death Dis 11: 574, 2020.
10. Wei J, Zhao Y, Liang H, Du W and Wang L: Preliminary evidence for the presence of multiple forms of cell death in diabetes cardiomyopathy. Acta Pharm Sin B 12: 1-17, 2022.
11. Bertheloot D, Latz E and Franklin BS: Necroptosis, pyroptosis and apoptosis: An intricate game of cell death. Cell Mol Immunol 18: 1106-1121, 2021.
12. Shi J, Gao W and Shao F: Pyroptosis: Gasdermin-mediated programmed necrotic cell death. Trends Biochem Sci 42: 245-254, 2017.
13. Kovacs SB and Miao EA: Gasdermins: Effectors of pyroptosis. Trends Cell Biol 27: 673-684, 2017.
14. Zhaolin Z, Guohua L, Shiyuan W and Zuo W: Role of pyroptosis in cardiovascular disease. Cell Prolif 52: e12563, 2019.
15. Bushati N and Cohen SM: microRNA functions. Annu Rev Cell Dev Biol 23: 175-205, 2017.
16. Lu TX and Rothenberg ME: MicroRNA. J Allergy Clin Immunol 141: 1202-1207, 2018.
17. Duygu B, de Windt LJ and da Costa Martins PA: Targeting microRNAs in heart failure. Trends Cardiovasc Med 26: 99-110, 2016.
18. Mohr AM and Mott JL: Overview of microRNA biology. Semin Liver Dis 35: 3-11, 2015.
19. Schulte C, Karakas M and Zeller T: microRNAs in cardiovascular disease-clinical application. Clin Chem Lab Med 55: 687-704, 2017.
20. He X, Kuang G, Wu Y and Ou C: Emerging roles of exosomal miRNAs in diabetes mellitus. Clin Transl Med 11: e468, 2021.
21. Xia Q, Wu F, Wu WB, Dong H, Huang ZY, Xu L, Lu FE and Gong J: Berberine reduces hepatic ceramide levels to improve insulin resistance in HFD-fed mice by inhibiting HIF-2α. Biomed Pharmacother 150: 112955, 2022.
22. Li G, Xing W, Zhang M, Geng F, Yang H, Zhang H, Zhang X, Li J, Dong L and Gao F: Antifibrotic cardioprotection of berberine via downregulating myocardial IGF-1 receptor-regulated MMP-2/MMP-9 expression in diabetic rats. Am J Physiol Heart Circ Physiol 315: H802-H813, 2018.

23. Cai L, Li W, Wang G, Guo L, Jiang Y and Kang YJ: Hyperglycemia-induced apoptosis in mouse myocardium: Mitochondrial cytochrome C-mediated caspase-3 activation pathway. Diabetes 51: 1938-1948, 2022.
24. Ren Z, Yu J, Wu Z, Si W, Li X, Liu Y, Zhou J, Deng R and Chen D: MicroRNA-210-5p contributes to cognitive impairment in early vascular dementia rat model through targeting Snap25. Front Mol Neurosci 11: 388, 2018.
25. Livak KJ and Schmittgen TD: Analysis of relative gene expression data using real-time quantitative PCR and the 2(-Delta Delta C(T)) method. Methods 25: 402-408, 2001.
26. Benetatos L and Vartholomatos G: Deregulated microRNAs in multiple myeloma. Cancer 118: 878-887, 2012.
27. Zhou B, Zhang JY, Liu XS, Chen HZ, Ai YL, Cheng K, Sun RY, Zhou D, Han J and Wu Q: Tom20 senses iron-activated ROS signaling to promote melanoma cell pyroptosis. Cell Res 28: 1171-1185, 2018.
28. Chang W, Zhang M, Meng Z, Yu Y, Yao F, Hatch GM and Chen L: Berberine treatment prevents cardiac dysfunction and remodeling through activation of 5'-adenosine monophosphate-activated protein kinase in type 2 diabetic rats and in palmitate-induced hypertrophic H9c2 cells. Eur J Pharmacol 769: 55-63, 2015.
29. Dong S, Zhang S, Chen Z, Zhang R, Tian L, Cheng L, Shang F and Sun J: Berberine could ameliorate cardiac dysfunction via interfering myocardial lipidomic profiles in the rat model of diabetic cardiomyopathy. Front Physiol 9: 1042, 2018.
30. Chang W, Zhang M, Li J, Meng Z, Wei S, Du H, Chen L and Hatch GM: Berberine improves insulin resistance in cardiomyocytes via activation of 5'-adenosine monophosphate-activated protein kinase. Metabolism 62: 1159-1167, 2013.
31. Tang M, Yuan D and Liao P: Berberine improves intestinal barrier function and reduces inflammation, immunosuppression, and oxidative stress by regulating the NF-κB/MAPK signaling pathway in deoxynivalenol-challenged piglets. Environ Pollut 289: 117865, 2021.
32. Xu J and Núñez G: The NLRP3 inflammasome: Activation and regulation. Trends Biochem Sci 48: 331-344, 2023.
33. Ha M and Kim VN: Regulation of microRNA biogenesis. Nat Rev Mol Cell Biol 15: 509-524, 2014.
34. Chamorro-Jorganes A, Sweaad WK, Katare R, Besnier M, Anwar M, Beazley-Long N, Sala-Newby G, Ruiz-Polo I, Chandrasekera D, Ritchie AA, *et al*: METTL3 regulates angiogenesis by modulating let-7e-5p and miRNA-18a-5p expression in endothelial cells. Arterioscler Thromb Vasc Biol 41: e325-e337, 2021.
35. Nandi SS, Katsurada K, Mahata SK and Patel KP: Neurogenic hypertension mediated mitochondrial abnormality leads to cardiomyopathy: Contribution of UPR^{mt} and norepinephrine-miR-18a-5p-HIF-1α axis. Front Physiol 12: 718982, 2021.
36. Zhu X, Bian H, Wang L, Sun X, Xu X, Yan H, Xia M, Chang X, Lu Y, Li Y, *et al*: Berberine attenuates nonalcoholic hepatic steatosis through the AMPK-SREBP-1c-SCD1 pathway. Free Radic Biol Med 141: 192-204, 2019.